

Evidence for a Superfluid-to-solid Transition of Bilayer Excitons

Yihang Zeng¹, Q. Shi¹, A. Okounkova¹, Dihao Sun¹, K.

Watanabe², T. Taniguchi³, J. Hone⁴, C.R. Dean^{1†}, and J.I.A. Li^{5†}

¹*Department of Physics, Columbia University, New York, NY 10027, USA*

²*Research Center for Electronic and Optical Materials,*

National Institute for Materials Science, 1-1 Namiki, Tsukuba 305-0044, Japan

³*Research Center for Materials Nanoarchitectonics,*

National Institute for Materials Science, 1-1 Namiki, Tsukuba 305-0044, Japan

⁴*Department of Mechanical Engineering, Columbia University, New York, NY 10027, USA*

⁵*Department of Physics, Brown University, Providence, RI 02912, USA and*

[†] *Email: cdean@phys.columbia.edu, jia.li@brown.edu*

(Dated: June 30, 2023)

The low-temperature phase diagram of a Bosonic system is predicted to contain an exotic quantum phase, called a supersolid, that is defined by broken translational symmetry and off-diagonal long-range order [1–5]. This unique combination of properties enables a seemingly paradoxical scenario where a bosonic solid exhibits dissipationless mass flow. However, despite decades of extensive efforts, experimental realization of such a supersolid phase remains elusive[6–8]. In this work we report experimental observation of a superfluid-to-insulating transition in the bosonic system of spatially indirect excitons in double layer graphene. Utilizing a variety of transport methods to characterize the superfluid-insulator phase boundary as a function of both density and temperature suggests the insulator to be a solid phase driven by repulsive dipole-dipole interactions in the dilute limit. The exciton solid exhibits a unique melting transition, with the high-temperature phase recovering a hallmark transport signature of off-diagonal long-range order, perfect Coulomb drag [9, 10]. The reentrant superfluid-like behaviour could indicate the low temperature solid also corresponds to a quantum coherent phase.

Following the experimental discovery of superfluid ⁴He [11, 12], it was theoretically proposed [2–5, 13] that there could also exist an exotic crystalline phase of helium at low temperature that simultaneously exhibits the properties of both a solid, such as broken translational symmetry, and a superfluid, such as zero viscosity. Termed a supersolid, its prediction motivated several decades of exhaustive research. However, experimental progress towards demonstrating this phase in ⁴He remains limited [6–8]. Recent advancements have been made in the context of cold atoms where coexisting superfluid properties and density modulation are observed [14–17]. Yet the original proposal where, due to repulsive interactions, a bosonic condensate with off-diagonal long-range order could also exhibit crystalline order with a single particle at each lattice site, remains unrealized.

Bilayer excitons have been identified as a promising system in which to realize the supersolid phase in a condensed-matter platform[18–25]. By spatially confining electrons and holes to closely separated, but electrically isolated, two-dimensional layers, a system of long-lived interlayer-excitons can be realized. Below a characteristic temperature dictated by the energetics of the system [26–29], the bosonic excitons can then undergo a Bose-Einstein condensation to a quantum-coherent ground state. Experimental evidence for the interlayer-exciton condensate has been demonstrated in GaAs, graphene, and transition metal dichalcogenide homo and hetero bilayers [9, 10, 30–39]. In all cases, the ground state is identified as a superfluid.

The low-temperature phase diagram of the bilayer-exciton condensate is theoretically defined by the interplay between three energy scales: interlayer attraction, E_{inter} , intra-layer repulsion, E_{intra} , and kinetic energy, E_k . The ratio E_{intra}/E_{inter} determines the pairing strength - the condensate forms in the limit where $E_{intra}/E_{inter} < 1$. The nature of this condensate is then determined by the ratio $E_{intra}/E_k = r_s$, where r_s is called the interaction parameter. For small r_s , the superfluid state is expected. A transition to solid phase occurs when the intralayer repulsion becomes dominant over the kinetic energy, $r_s \gg 1$. Although this phase diagram has been studied theoretically, tuning the relevant energy scales presents an experimental challenge and only a limited region of phase space has been explored. To date, no evidence of an exciton superfluid-to-insulator transition has been reported.

We address this challenge by studying magneto-bilayer excitons in the quantum Hall regime. In symmetrically doped quantum Hall bilayers, electrons in a partially filled Landau level (LL) in one layer couple with vacancies in the other to form bound excitons (Fig. 1a). The interlayer attraction is inversely proportional to the layer spacing, $E_{inter} \sim 1/d$, whereas the intralayer repulsion is determined by the magnetic length, $E_{intra} \sim 1/\ell_B$, with $\ell_B \propto 1/\sqrt{B}$, so that the condensate regime is defined by $E_{intra}/E_{inter} \propto d/\ell_B$. The dimensionless parameter d/ℓ_B is tunable with magnetic field, providing a way to

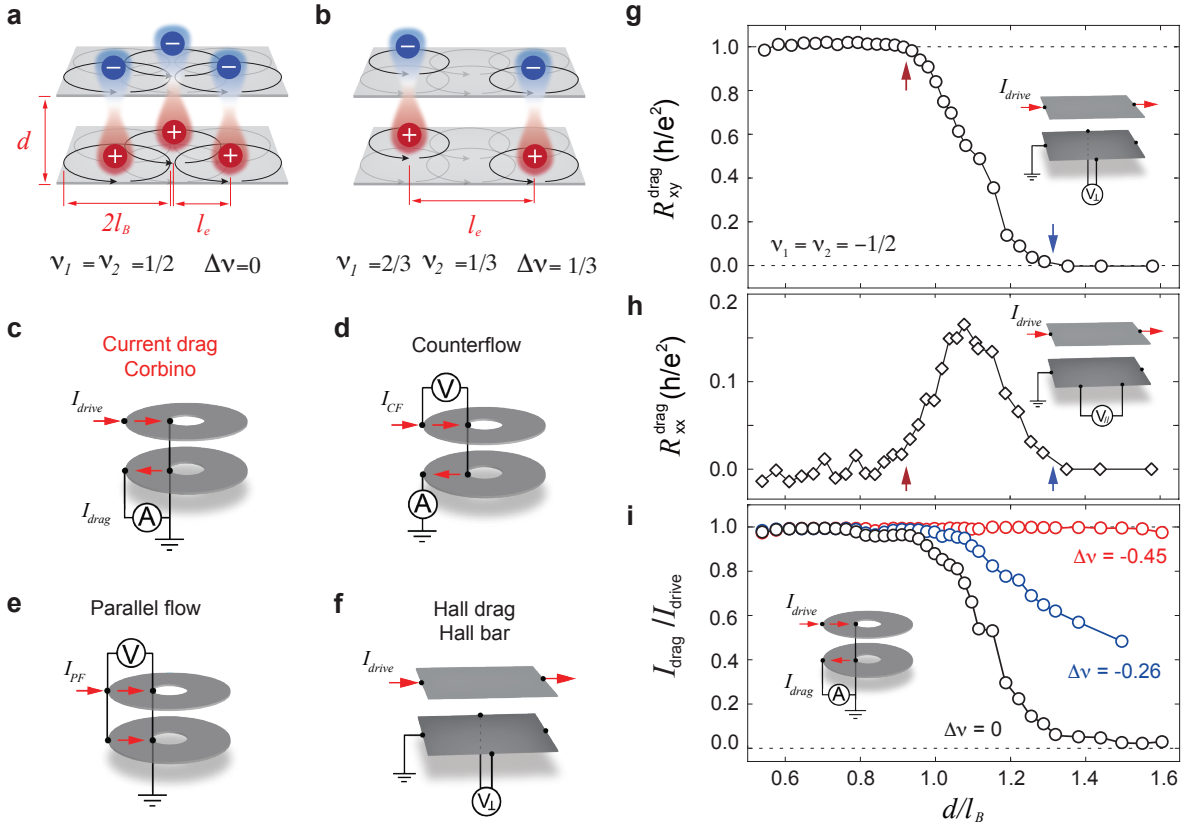


FIG. 1. **Transport signatures of the Exciton condensate.** (a-b) Schematics diagram of interlayer excitons in a quantum Hall bilayer system at $\nu_{\text{total}} = 1$. ℓ_B denotes the magnetic length, whereas ℓ_e corresponds to the average spacing between excitons. (a) The ratio of ℓ_e/ℓ_B is minimized under the layer balanced condition $\nu_1 = \nu_2 = 1/2$. (b) The effective exciton density is reduced in the presence of layer imbalance, giving rise to an enhanced ℓ_e/ℓ_B . (e-f) Schematic diagram for the sample geometry and measurement configuration of various transport methods. (c) Current drag, (d) counterflow, (e) parallel flow measurements are performed in samples with Corbino-shape, whereas (f) Hall drag measurement is performed in samples with a hall bar shape. (g) Hall drag, (h) longitudinal drag, and (i) Current drag ratio $I_{\text{drag}}/I_{\text{drive}}$ as a function of effective interlayer separation d/ℓ_B . Black circles and diamonds denote measurements under the layer-balanced condition $\Delta\nu = 0$, whereas blue and red circles are measured with an imbalance between the Landau level fillings across two layers. All measurements are measured at $T = 0.3$ K in samples with the interlayer separation of $d = 7.4$ nm.

adjust the exciton pairing strength in a device with fixed layer separation. Studies of quantum Hall bilayers have confirmed that the magneto-exciton condensate onsets for $d/\ell_B < 1$ [9, 10, 30–39], with a crossover from weak-pairing to strong-pairing superfluid transition observed as d/ℓ_B is tuned from 1 to 0 [36].

In principle, accessing the exciton solid phase requires achieving a large value of r_s . However, in the quantum Hall regime this quantity is ill-defined, since the kinetic energy is quenched. One might consider that $r_s \rightarrow \infty$ and therefore the exciton solid criterion is naturally met. However, the fact that no evidence of an exciton solid has been found in quantum Hall bilayers instead indicates that r_s is not the relevant parameter for magneto-excitons. In this work, we identify a new parameter, ℓ_e , that defines the average distance between excitons. The inter-particle distance within a layer relates to the carrier density, n , according to $n_i = 1/\pi\ell_e^2 = \nu_i/\pi\ell_B^2$, where ν_i

is the LL filling fraction and i is the layer index. When the two layers are balanced with both tuned to half filling (Fig. 1a) the inter-exciton spacing is $\ell_e = \sqrt{2}\ell_B$. When the layers are imbalanced, while maintaining total filling fraction $\nu_{\text{tot}} = 1$, we define the exciton density by the minority carrier filling fraction (Fig. 1b). This gives (see SI), $\ell_e = \ell_B/\sqrt{1/2 - |\Delta\nu|/2}$ where $\Delta\nu = \nu_1 - \nu_2$. Thus, at layer-balance ($\Delta\nu = 0$), which has been the focus of past experimental efforts, ℓ_e is minimized (Fig. 1a). However, under imbalance, ℓ_e increases with $\Delta\nu$. Here we observe a superfluid-to-insulator transition upon tuning $\Delta\nu$ to achieve ℓ_e/ℓ_B above a critical value. Examination of the temperature and ℓ_e/ℓ_B -tuned phase transitions provide hints that the insulating phase could be a realization of the long-predicted bosonic supersolid.

We study interlayer magneto-excitons in heterostructures consisting of two graphene monolayers separated by a multi-layer hBN spacer [36, 40, 41]. Several de-

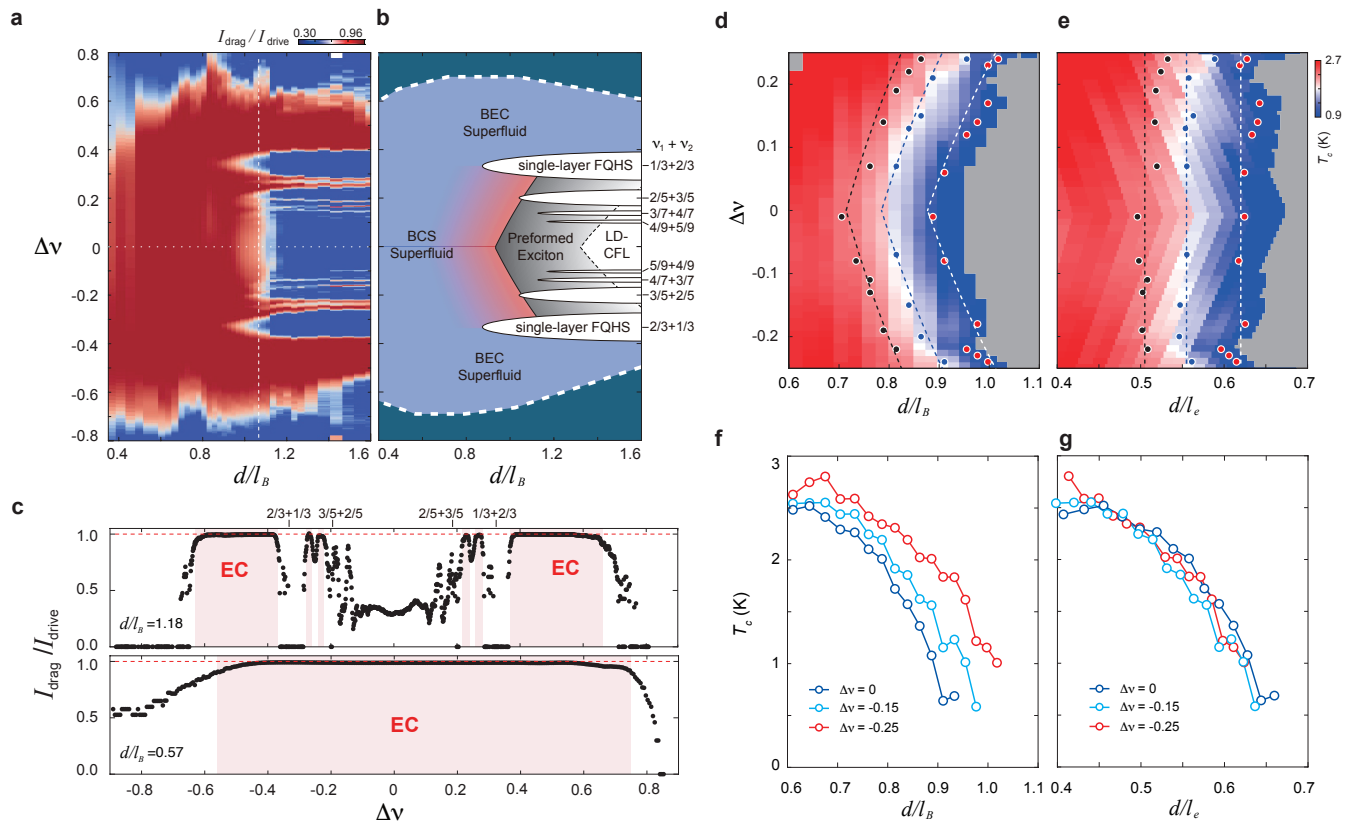


FIG. 2. **The condensate phase with inter-exciton spacing ℓ_e .** (a) Current drag ratio I_{drag}/I_{drive} as a function of layer-imbalance $\Delta\nu$ and effective interlayer separation d/ℓ_B . The exciton condensate phase with perfect drag ratio $I_{drag}/I_{drive} = 1$ is shown as red in the chosen color scale. The layer decoupled phase exhibits zero drag ratio, which is shown as blue. (b) Schematic diagram of the $\Delta\nu$ - d/ℓ_B map. Layer-decoupled fractional quantum Hall states are labeled based on the LL filling of each layer. For instance, $1/3 + 2/3$ indicates the Laughlin state at $\nu_1 = 1/3$ and $\nu_2 = 2/3$. (c) Current drag ratio I_{drag}/I_{drive} as a function of $\Delta\nu$ measured at $d/\ell_B = 1.18$ (top panel) and $d/\ell_B = 0.57$ (bottom panel). Red stripes indicate regions of perfect drag response. Minima in the upper panel correspond to the FQHE sequence labelled in (b). LL filling of each layer is marked near the top axis. T_c as a function of (d) $\Delta\nu$ and d/ℓ_B , (e) $\Delta\nu$ and d/ℓ_e . Constant values of T_c are marked by black, blue and red circles. T_c as a function of (f) d/ℓ_B and (g) d/ℓ_e measured at different interlayer density imbalance $\Delta\nu$. T_c is operationally defined as the temperature at which Hall drag response equals 98% of the quantized plateau, $R_{xy}^{drag} = 0.98h/e^2$ (also see Fig. S2).

vice configurations are utilized, shown in Fig. 1c-f. The Coulomb drag measurement in Corbino-shaped devices [9, 40] allows us to directly probe the exciton transport without the influence of the edge states. When the current bias I_{drive} is entirely carried by the exciton drag current I_{drag} , perfect drag response, $I_{drag}/I_{drive} = 1$, offers a hallmark signature of the off-diagonal long range order and is regarded as an unambiguous identification of the exciton condensate phase [9, 10]. A condensate phase is expected to be highly conductive in the counterflow measurement (Fig. 1d), but insulating in parallel flow (Fig. 1e). In the Hall bar geometry (Fig. 1f), the exciton condensate phase exhibits quantized Hall drag R_{xy}^{drag} , concomitant with vanishing longitudinal drag response [34–36]. All devices include a top and bottom gate (not shown) to allow independent density tuning in each layer.

Fig. 1g-i displays the evolution of the exciton condensate phase as a function of d/ℓ_B . At small d/ℓ_B , and layer balance, the condensate phase exhibits a quantized plateau in the Hall drag response R_{xy}^{drag} (Fig. 1g), diminishing longitudinal drag R_{xx}^{drag} (Fig. 1h), as well as the perfect drag response with $I_{drag}/I_{drive} = 1$ (Fig. 1i). In the limit of $d/\ell_B > 1$, both Hall drag and current drag responses reduce to zero indicating a transition to a layer-decoupled phase at large d/ℓ_B . Longitudinal drag is zero-valued for both the interlayer-coherent and layer-decoupled regimes, but peaks at the transition between them [42]. Under layer imbalance, the transition from the condensate to a layer-decoupled phase shifts to larger d/ℓ_B (Fig. 1i), suggesting that the stability of the exciton condensate phase is enhanced in the presence of layer imbalance [43].

Fig. 2a shows a colour plot of the current drag re-

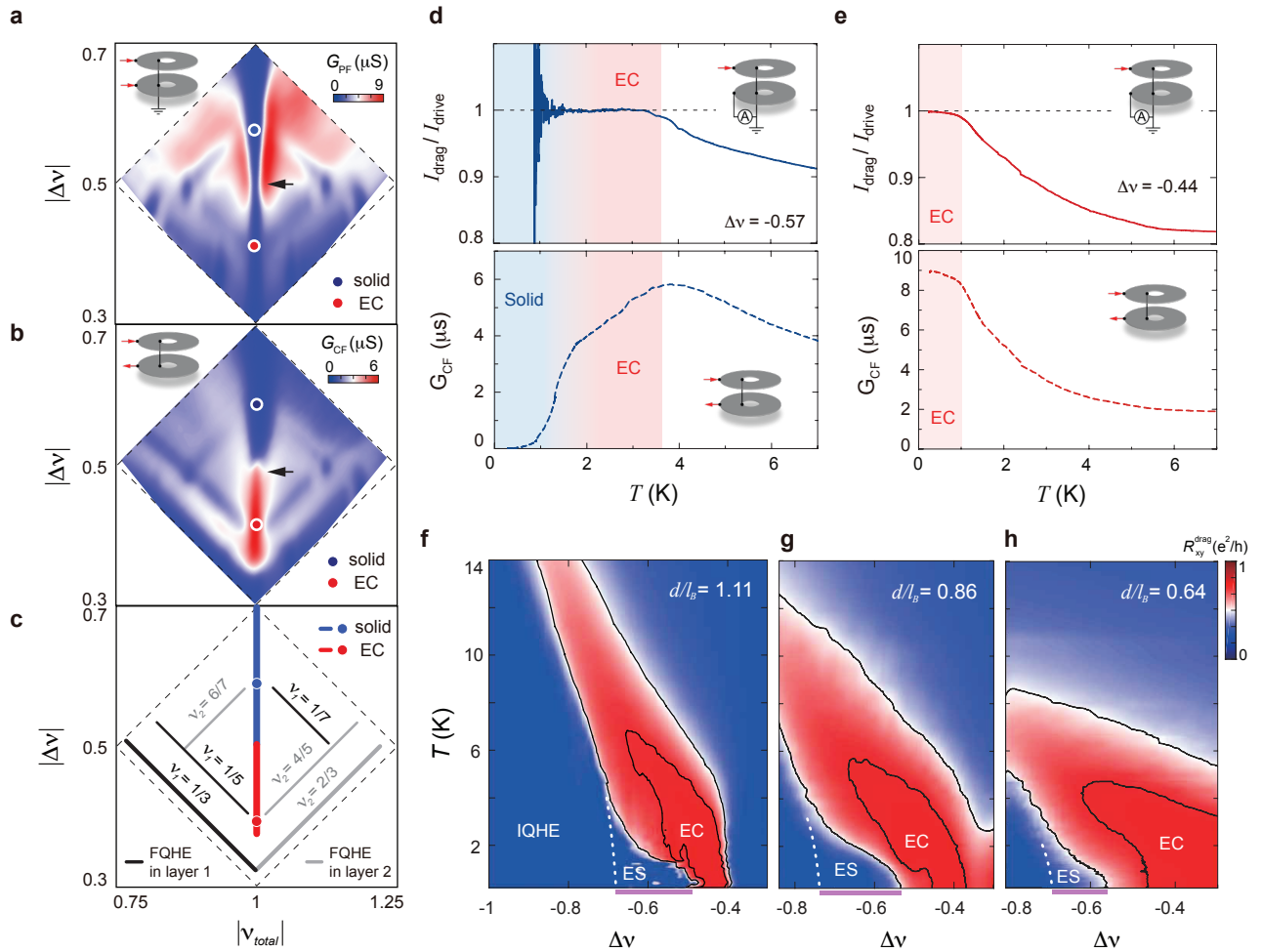


FIG. 3. **The exciton solid.** (a-b) Counterflow and parallel flow response near the transition boundary between the condensate and single-layer IQHS. (a) parallel flow conductance G_{PF} and (b) Counterflow conductance G_{CF} as a function of total Landau level filling ν_{total} and layer imbalance $\Delta\nu$. The measurement is performed at $d/\ell_B = 1.6$. (c) Schematic diagram labeling the most prominent features in panels (a) and (b). (d-e) The temperature dependence of drag ratio I_{drag}/I_{drive} (top panel) and Counterflow conductance G_{CF} (bottom panel) for (d) the exciton solid state at $\Delta\nu = -0.57$, and (e) the exciton condensate at $\Delta\nu = -0.44$. The location of the condensate and solid phases in the $\nu_{total}-\Delta\nu$ map are marked by red and blue circles in panels (a) and (b). (f-h) Hall drag as a function of temperature T and layer imbalance $\Delta\nu$ measured at different values of d/ℓ_B . The measurement is performed at $\nu_{total} = 1$. The regime occupied by the condensate phase, marked by *EC*, is defined by the contour of Hall drag response at $R_{xy}^{drag} = 0.98h/e^2$. The *EC* regime displays a unique “wing” shape in the $\Delta\nu - T$ map, revealing an exciton solid as the intermediate phase at the condensate-to-IQHS transition.

sponse versus $\Delta\nu$ and d/ℓ_B . For $d/\ell_B < 1$, a large portion of the phase space is occupied by the condensate phase, evidenced by the perfect Coulomb drag response with $I_{drive}/I_{drag} = 1$ (shown as red in the chosen color scale). For $d/\ell_B > 1$, the condensate disappears at $\Delta\nu = 0$ (blue color), but reappears under layer balance. We note, however, that it is periodically interrupted by a sequence of zero drag regions (blue horizontal stripes) that correspond in filling fraction to the expected single layer FQHE states. The competition between the exciton condensate and single-layer FQHE is further illustrated by the $\Delta\nu$ -dependence of the current drag response measured at a fixed d/ℓ_B , as shown in Fig. 2c. Hall bar

measurement confirms (see SI) that that upon increasing layer imbalance, the *EC* exhibits a d/ℓ_B dependent competition with incompressible single-layer FQHE states. The competition between the bilayer condensate and single layer FQHE states under layer imbalance has not, to our knowledge, been previously examined and merits future study.

The enhancement of the condensate with increasing $\Delta\nu$ is dramatic. As shown in Fig. 2a-b, perfect Coulomb drag response persists beyond $d/\ell_B = 1.6$ for $|\Delta\nu| > 0.4$. To examine this quantitatively, Fig. 2d plots T_c versus $\Delta\nu$ and d/ℓ_B . We restrict to regime $|\Delta\nu| < 0.2$ to avoid influence of the competition with the single-layer

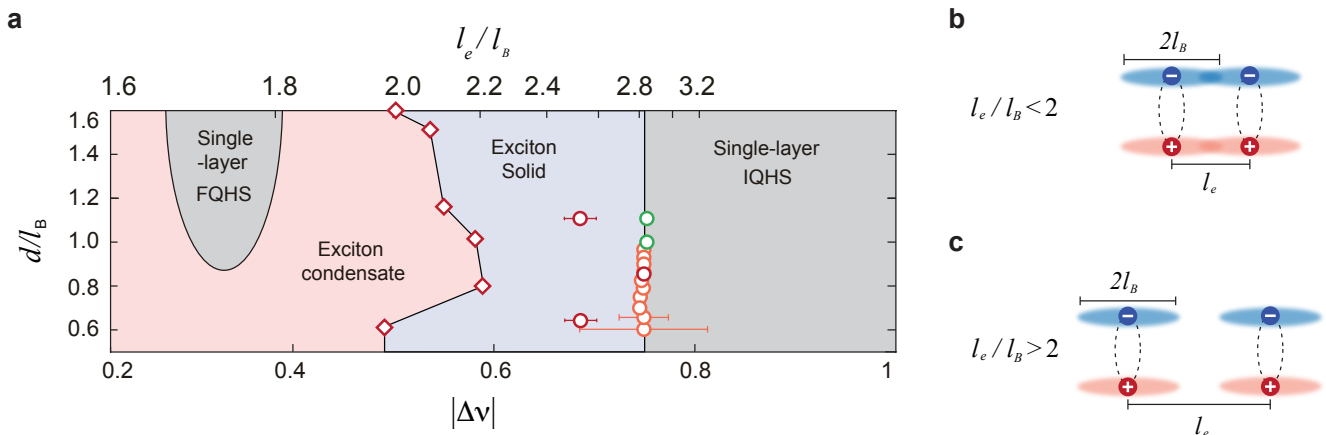


FIG. 4. **The scaling argument.** (a) Schematic phase diagram of the $\Delta\nu - d/\ell_B$ map showing various exciton phases and associate phase boundaries at $\nu_{total} = 1$. The location of the superfluid-to-solid transition is identified based on the current drag and counterflow measurements in Fig. 3, whereas the transition between the exciton solid and single-layer IQHS is determined based on the temperature dependence of the counterflow and drag responses (see Fig. S7 and the SI). (b) The exciton superfluid-solid transition with the scaling argument. $R_C = \ell_B$ is the cyclotron radius of charge carriers in the lowest Landau level. According to the scaling argument, an exciton solid phase is expected to be stabilized when $\ell_e > 2R_C$ is satisfied. Whereas a superfluid phase is stable at $\ell_e < 2R_C$.

FQHE states. White and red circles mark constant values of T_c , which we take as a reflection of the stability of the exciton condensate. For a given value of d/ℓ_B , T_c is enhanced by increasing $\Delta\nu$. A similar trend is observed in the superfluid transition width, ΔT (see SI).

The observation that T_c and ΔT vary with $\Delta\nu$, for fixed d/ℓ_B , suggests that d/ℓ_B alone does not fully describe the ground state of the bosonic system. Fig. 2e replots the same T_c , but as a function of $\Delta\nu$ and d/ℓ_e , where ℓ_e is calculated from the definition of above. The contours of constant T_c now follow vertical trajectories, which is a strong indication that the excitonic pairing strength is fully determined by d/ℓ_e and independent of layer imbalance. Likewise, the measured T_c follows distinct trajectories for different values of $\Delta\nu$ when plotted as a function of d/ℓ_B (Fig. 2f) but the same data collapse onto a single curve when plotted as a function of d/ℓ_e - confirming that ℓ_e , and therefore the exciton density, plays a critical role in determining the stability of the condensate phase. This provides a physical picture that links the magneto-exciton phase diagram with the previously studied zero-field bilayer excitons.

Next we consider the nature of the condensate under large layer imbalance, corresponding to the dilute regime of low-density excitons. The dashed line in fig. 2b marks a value of large $|\Delta\nu|$ that separates two excitonic behaviours. Inside this boundary we observe perfect drag indicating superfluid excitons. Outside this boundary the system transitions to a phase that exhibits zero drag response. In Fig. 3a and b we examine this apparent phase boundary in more detail by plotting high resolution maps of parallel-flow and counterflow conductance,

respectively, versus total filling fraction, ν_{total} (horizontal axis) and layer imbalance, $\Delta\nu$ (vertical axis). The data was acquired at $d/\ell_B = 1.6$ from the same Corbino device as in Fig. 2. The exciton condensate is maintained only at $|\nu_{total}| = 1$, and therefore follows a vertical trajectory through the center of these maps [10, 34, 35, 39, 40, 44]. The black arrows in Figs. 3a,b identify a transition boundary that occurs around $\Delta\nu = 0.5$. For $\Delta\nu < 0.5$, the device shows vanishing conductance in parallel flow (blue in Fig. 3a) but high conductance in counterflow (red in Fig 3b), consistent with the expected response for superfluid bilayer excitons. For $\Delta\nu > 0.5$, the device shows vanishing conductance in both parallel and counterflow. That the high $\Delta\nu$ feature continues to evolve along $\nu_{total} = 1$ and shows zero parallel flow conductance, indicates that it continues to reflect an interlayer exciton state. The transition to zero-value counterflow conductance indicates that the $\nu = 0.5$ phase boundary identifies an exciton-superfluid to exciton-insulator phase boundary.

Since the superfluid-to-insulator transition is located near the edge of the Landau level, a natural question is whether the insulating phase is driven by disorder-induced localization [45]. We note that when ν_{total} is slightly detuned away from $\nu_{total} = 1$, the exciton pairs dissociate and the insulator is replaced by a layer-decoupled metallic phase, which is highly conductive in both parallel flow and counterflow measurements (Fig. 3a-c). This indicates that if disorder localization is at play, it must be of a peculiar type that affects excitons but not individual-layer charge carriers.

Fig. 3d shows the temperature dependence of the cur-

rent drag, and counterflow conductance, of the exciton insulator, measured in the Corbino device at $\Delta\nu = 0.56$ and $d/\ell_B = 1.6$. For $T \lesssim 1.5\text{K}$, the insulator is evidenced by zero counterflow conductance, $G_{CF} = 0$ (Fig. 3d lower panel). Since the drive current is vanishingly small, the current drag ratio I_{drag}/I_{drive} , is ill-defined (Fig. 3d upper panel). With increasing T , the counterflow conductance becomes non-zero at $T \sim 1.5\text{K}$, rises to a peak value near $T \sim 4\text{K}$ and then slowly decreases with increasing temperature. This non-monotonic temperature dependence is reminiscent of the melting transition of an electronic Wigner solid, where the conductance peak defines the melting temperature [46–51]. Coincident with the onset of a finite counterflow conductance, the current drag recovers a perfect drag response at around $T \sim 1.5\text{K}$ that persists to $\sim 4\text{K}$. The combined drag and counterflow behaviours are in stark contrast with that of the superfluid condensate behaviour, such as shown in Fig. 3e, where, beyond a critical temperature, both current drag and counterflow conductance of the EC phase decrease monotonically.

The reentrant-type transition is corroborated by the Hall drag measurement from Hall-bar samples. Fig. 3f-h plots the Hall drag response as a function of temperature T and layer imbalance $\Delta\nu$, acquired at three different values of d/ℓ_B . The $\Delta\nu$ -range of the exciton insulator, identified from Fig. 3a-c, is highlighted by purple horizontal stripes near the bottom axis. In the chosen color scale, red denotes quantized Hall drag response with a plateau value of e^2/h . According to the $\Delta\nu - T$ map, the exciton condensate phase with quantized Hall drag occupies a wing-shaped regime. At low temperature, quantized Hall drag is absent in the range of the exciton insulator, but it re-appears with increasing T , consistent with what was observed in the current drag and counterflow response of the corbino device (Fig. 3d).

A re-entrance from an exciton insulator to a conducting state with characteristic superfluid properties, upon raising the temperature, has intriguing implications. Since the low-temperature phase is less entropic, the free energy of the exciton insulator must be lower than the apparent superfluid phase that is recovered upon heating. This scenario challenges the conventional perception, which is implied by the two-fluid model, that a superfluid condensate always persists to zero-temperature [52–54]. Furthermore, perfect current drag and quantized Hall drag point towards a Berezinskii-Kosterlitz-Thouless (BKT) type order, which establishes the presence of off-diagonal long range order at high temperature [55, 56]. This makes disorder localization an unlikely mechanism for the insulating state at low temperature [57]. Alternatively, the low temperature insulating phase could indicate the formation of an exciton solid, where the crystalline order breaks translational symmetry [58]. In this scenario, the insulating to conducting transition with increasing temperature marks the melt-

ing transition of the exciton solid. The appearance of a superfluid condensate above the melting temperature suggests that the proposed solid phase is distinct from a bilayer Wigner crystal, where electronic solids in the two layers form independently with weak interlayer correlation [23, 59–61] since any layer-decoupled state would be expected to exist at a higher temperature compared to an interlayer correlated condensate.

An alternate interpretation of the reentrant superfluid behaviour is that this results from a temperature-induced de-pinning of the solid phase. In this scenario, signatures of interlayer coherence and long range order, such as perfect drag and quantized Hall drag, in the temperature window $1.5 < T < 4\text{K}$, coexist with a persistent solid phase, and the melting transition occurs at $T > 4\text{K}$. Such coexistence would be strong evidence for a super-solid phase. While this scenario is consistent with our observation, we note that transport measurement alone does not offer definitive identification of a supersolid. Yet another possibility for the reentrance is that above 1.5K the system enters into a mixed phase with coexisting solid and superfluid condensate phases, with transition to normal state onset above 4K . Again however, the existence of a solid phase appearing at a lower temperature than the superfluid likely requires a non-trivial explanation. Further theoretical and experimental work will be necessary to fully resolve the nature of both the ground state of the insulator and the observed temperature dependence.

Fig. 4a plots a select region of the low temperature phase diagram summarizing the various phases we access by tuning d/ℓ_B and $|\Delta\nu|$. We plot $\Delta\nu$ along the bottom axis, and identify the associated value of ℓ_e/ℓ_B along the top axis. We note the striking result that throughout the experimentally accessible range of d/ℓ_B , the superfluid-to-insulator transition around $\ell_e/\ell_B \sim 2$. This defines a natural length scale for the transition in terms of the exciton density, coinciding with the point at which the exciton-exciton spacing exceeds the intralayer Coulomb interaction length scale, defined by ℓ_B (Fig. 4b,c). If we consider ℓ_B to define the Bohr radius for magneto-excitons, then our observation suggests that at low temperature, the insulator is stabilized when the exciton spacing exceeds the Bohr radius, and the repulsive interaction transitions from being dominated by intralayer Coulomb to, dipole-dipole interaction. We note that this resembles a similar scaling argument that identified the Wigner crystal forms in the QHE regime of single layer quantum wells in the dilute limit [62–66], where the electron-electron spacing exceeds the magnetic length [38, 48].

To conclude, we report observation of an exciton superfluid-to-insulator transition in quantum Hall bilayers. The insulator is stabilized at low temperature by tuning layer imbalance to reach the low exciton density regime. An unexpected reentrant superfluid behaviour is

observed upon heating the solid, establishing an intriguing relationship between the solid phase and dissipationless exciton flow. While the nature of the solid phase and the associated melting transition are not fully understood, the unprecedented tunability available in quantum Hall bilayers offers wide-ranging opportunities to address this question in future experiments. Finally, our measurements unambiguously confirm the theoretical prediction that a bilayer condensate can transition to an insulating phase in the dilute limit [18, 25]. We anticipate this result will guide efforts to access similar states in zero-field bilayer heterostructures [19, 29, 67, 68].

ACKNOWLEDGMENTS

J.I.A.L. and C.R.D. wish to thank Sankar Das Sarma and Kun Yang for stimulating discussions. This research was primarily supported by the US Department of Energy, Office of Science, Basic Energy Sciences, under award no. DE-SC0019481 (transport measurements). Heterostructure and device fabrication was supported by the NSF MRSEC program at Columbia through the Center for Precision-Assembled Quantum Materials (DMR-2011738). Data analysis (Q.S.) was partially supported by Department of Energy (DE-SC0016703). J.I.A.L. acknowledges support from the Sloan research fellowship. K.W. and T.T. acknowledge support from the JSPS KAKENHI (Grant Numbers 20H00354, 21H05233 and 23H02052) and World Premier International Research Center Initiative (WPI), MEXT, Japan. A portion of this work was performed at the National High Magnetic Field Laboratory, which is supported by National Science Foundation Cooperative Agreement No. DMR-1157490 and the State of Florida.

COMPETING FINANCIAL INTERESTS

The authors declare no competing financial interests.

-
- [1] M. P. A. Fisher, P. B. Weichman, G. Grinstein, and D. S. Fisher, *Phys. Rev. B* **40**, 546 (1989).
- [2] O. Penrose and L. Onsager, *Phys. Rev.* **104**, 576 (1956).
- [3] A. Andreev and I. Lifshits, *Zhur Eksper Teoret Fiziki* **56**, 2057 (1969).
- [4] A. J. Leggett, *Phys. Rev. Lett.* **25**, 1543 (1970).
- [5] M. W. Meisel, *Physica B: Condensed Matter* **178**, 121 (1992).
- [6] E. Kim and M. H. Chan, *Science* **305**, 1941 (2004).
- [7] J. Day and J. Beamish, *Nature* **450**, 853 (2007).
- [8] B. Hunt, E. Pratt, V. Gadagkar, M. Yamashita, A. V. Balatsky, and J. Davis, *Science* **324**, 632 (2009).
- [9] D. Nandi, A. D. K. Finck, J. P. Eisenstein, L. N. Pfeiffer, and K. W. West, *Nature* **488**, 481 (2012).
- [10] J. P. Eisenstein, *Annu. Rev. of Condens. Matter Phys.* **5**, 159 (2014).
- [11] J. F. Allen and A. Misener, *Nature* **142**, 643 (1938).
- [12] P. Kapitza, *Nature* **141**, 74 (1938).
- [13] G. V. Chester, *Phys. Rev. A* **2**, 256 (1970).
- [14] L. Tanzi, E. Lucioni, F. Famà, J. Catani, A. Fioretti, C. Gabbanini, R. N. Bisset, L. Santos, and G. Modugno, *Physical review letters* **122**, 130405 (2019).
- [15] L. Chomaz, D. Petter, P. Ilzhöfer, G. Natale, A. Trautmann, C. Politi, G. Durastante, R. Van Bijnen, A. Patscheider, M. Sohmen, *et al.*, *Physical Review X* **9**, 021012 (2019).
- [16] F. Böttcher, J.-N. Schmidt, M. Wenzel, J. Hertkorn, M. Guo, T. Langen, and T. Pfau, *Physical Review X* **9**, 011051 (2019).
- [17] M. A. Norcia, C. Politi, L. Klaus, E. Poli, M. Sohmen, M. J. Mark, R. N. Bisset, L. Santos, and F. Ferlaino, *Nature* **596**, 357 (2021).
- [18] Y. N. Joglekar, A. V. Balatsky, and S. D. Sarma, *Physical Review B* **74**, 233302 (2006).
- [19] S. Conti, A. Perali, A. R. Hamilton, M. V. Milošević, F. m. c. M. Peeters, and D. Neilson, *Phys. Rev. Lett.* **130**, 057001 (2023).
- [20] S. De Palo, F. Rapisarda, and G. Senatore, *Physical review letters* **88**, 206401 (2002).
- [21] M. Zarenia, D. Neilson, and F. Peeters, *Scientific reports* **7**, 1 (2017).
- [22] S. Chui, N. Wang, and C. Y. Wan, *Physical Review B* **102**, 125420 (2020).
- [23] D. Yoshioka and A. H. MacDonald, *Journal of the Physical Society of Japan* **59**, 4211 (1990).
- [24] X. Chen and J. Quinn, *Physical review letters* **67**, 895 (1991).
- [25] K. Yang, *Physical Review Letters* **87**, 056802 (2001).
- [26] Y. E. Lozovik and V. Yudson, *JETP Lett.* **22**, 274 (1975).
- [27] Y. E. Lozovik and V. Yudson, *JETP Lett.* **44**, 389 (1976).
- [28] J. M. Blatt, K. W. Böer, and W. Brandt, *Phys. Rev.* **126**, 1691 (1962).
- [29] M. Fogler, L. Butov, and K. Novoselov, *Nature communications* **5**, 4555 (2014).
- [30] M. Kellogg, J. P. Eisenstein, L. N. Pfeiffer, and K. W. West, *Phys. Rev. Lett.* **93**, 036801 (2004).
- [31] M. J. Kellogg, *Evidence for Excitonic Superfluidity in a Bilayer Two-Dimensional Electron System*, Ph.D. thesis, California Institute of Technology (2005).
- [32] E. Tutuc, M. Shayegan, and D. A. Huse, *Phys. Rev. Lett.* **93**, 036802 (2004).
- [33] R. D. Wiersma, J. G. S. Lok, S. Kraus, W. Dietsche, K. von Klitzing, D. Schuh, M. Bichler, H.-P. Tranitz, and W. Wegscheider, *Phys. Rev. Lett.* **93**, 266805 (2004).
- [34] J. I. A. Li, T. Taniguchi, K. Watanabe, J. Hone, and C. R. Dean, *Nat. Phys.* **13**, 751 (2017).
- [35] X. Liu, T. Taniguchi, K. Watanabe, B. Halperin, and P. Kim, *Nat. Phys.* **13**, 746 (2017).
- [36] X. Liu, J. Li, K. Watanabe, T. Taniguchi, J. Hone, B. I. Halperin, P. Kim, and C. R. Dean, *Science* **375**, 205 (2022).
- [37] G. W. Burg, N. Prasad, K. Kim, T. Taniguchi, K. Watanabe, A. H. MacDonald, L. F. Register, and E. Tutuc, *Phys. Rev. Lett.* **120**, 177702 (2018).
- [38] Q. Shi, E.-M. Shih, M. V. Gustafsson, D. Rhodes, B. Kim, K. Watanabe, T. Taniguchi, Z. Papić, J. Hone, and C. R. Dean, *Nature Nanotechnology* **15**, 569 (2020).

- [39] Q. Shi, E.-M. Shih, D. Rhodes, B. Kim, K. Barmak, K. Watanabe, T. Taniguchi, Z. Papić, D. A. Abanin, J. Hone, and C. R. Dean, *Nature Nanotechnology* **17**, 577 (2022).
- [40] J. Li, Q. Shi, Y. Zeng, K. Watanabe, T. Taniguchi, J. Hone, and C. Dean, *Nature Physics* **15**, 898 (2019).
- [41] X. Liu, Z. Hao, K. Watanabe, T. Taniguchi, B. I. Halperin, and P. Kim, *Nature Physics* **15**, 893 (2019).
- [42] M. Kellogg, J. P. Eisenstein, L. N. Pfeiffer, and K. W. West, *Phys. Rev. Lett.* **90**, 246801 (2003).
- [43] I. B. Spielman, M. Kellogg, J. P. Eisenstein, L. N. Pfeiffer, and K. W. West, *Phys. Rev. B* **70**, 081303 (2004).
- [44] J. P. Eisenstein and A. H. MacDonald, *Nature* **432**, 691 (2004).
- [45] S. Ahn and S. Das Sarma, *Phys. Rev. B* **107**, 195435 (2023).
- [46] E. Wigner, *Phys. Rev.* **46**, 1002 (1934).
- [47] M. M. Fogler, A. A. Koulakov, and B. I. Shklovskii, *Phys. Rev. B* **54**, 1853 (1996).
- [48] M. Goerbig and C. M. Smith, *EPL (Europhysics Letters)* **63**, 736 (2003).
- [49] I. L. Drichko, I. Y. Smirnov, A. V. Suslov, L. N. Pfeiffer, K. W. West, and Y. M. Galperin, *Phys. Rev. B* **92**, 205313 (2015).
- [50] S. Chen, R. Ribeiro-Palau, K. Yang, K. Watanabe, T. Taniguchi, J. Hone, M. O. Goerbig, and C. R. Dean, *Physical review letters* **122**, 026802 (2019).
- [51] H. Zhou, H. Polshyn, T. Taniguchi, K. Watanabe, and A. Young, *Nature Physics* **16**, 154 (2020).
- [52] F. London, *Physical Review* **54**, 947 (1938).
- [53] N. Bogoliubov, *J. Phys* **11**, 23 (1947).
- [54] A. Griffin, D. Snoke, and S. Stringari, “Bose-einstein condensation cambridge univ,” (1995).
- [55] V. Berezinskii, *Sov. Phys. JETP* **34**, 610 (1972).
- [56] J. M. Kosterlitz and D. J. Thouless, *Journal of Physics C: Solid State Physics* **6**, 1181 (1973).
- [57] D. S. L. Abergel, M. Rodriguez-Vega, E. Rossi, and S. Das Sarma, *Phys. Rev. B* **88**, 235402 (2013).
- [58] D. Vu and S. D. Sarma, *arXiv preprint arXiv:2305.16305* (2023).
- [59] Y. Zhou, J. Sung, E. Brutschea, I. Esterlis, Y. Wang, G. Scuri, R. J. Gelly, H. Heo, T. Taniguchi, K. Watanabe, *et al.*, *Nature* **595**, 48 (2021).
- [60] M. Zarenia, D. Neilson, and F. Peeters, *Scientific Reports* **7**, 11510 (2017).
- [61] Y. Zeng, Z. Xia, R. Dery, K. Watanabe, T. Taniguchi, J. Shan, and K. F. Mak, *Nature Materials* , 1 (2023).
- [62] E. Andrei, G. Deville, D. Glatli, F. Williams, E. Paris, and B. Etienne, *Physical review letters* **60**, 2765 (1988).
- [63] H. W. Jiang, R. L. Willett, H. L. Stormer, D. C. Tsui, L. N. Pfeiffer, and K. W. West, *Phys. Rev. Lett.* **65**, 633 (1990).
- [64] M. K. Ma, K. V. Rosales, H. Deng, Y. Chung, L. Pfeiffer, K. West, K. Baldwin, R. Winkler, and M. Shayegan, *Physical review letters* **125**, 036601 (2020).
- [65] G. Gervais, L. W. Engel, H. L. Stormer, D. C. Tsui, K. W. Baldwin, K. W. West, and L. N. Pfeiffer, *Phys. Rev. Lett.* **93**, 266804 (2004).
- [66] V. J. Goldman, M. Santos, M. Shayegan, and J. E. Cunningham, *Phys. Rev. Lett.* **65**, 2189 (1990).
- [67] Z. Wang, D. A. Rhodes, K. Watanabe, T. Taniguchi, J. C. Hone, J. Shan, and K. F. Mak, *Nature* **574**, 76 (2019).
- [68] L. Ma, P. X. Nguyen, Z. Wang, Y. Zeng, K. Watanabe, T. Taniguchi, A. H. MacDonald, K. F. Mak, and J. Shan, *Nature* **598**, 585 (2021).
- [69] M. Randeria and E. Taylor, *Annual Review of Condensed Matter Physics* **5**, 209 (2014).
- [70] A. Stern and B. I. Halperin, *Phys. Rev. Lett.* **88**, 106801 (2002).
- [71] S. H. Simon, E. H. Rezayi, and M. V. Milovanovic, *Phys. Rev. Lett.* **91**, 046803 (2003).

SUPPLEMENTARY MATERIALS

Evidence for a Superfluid-to-solid Transition of Bilayer Excitons

Yihang Zeng, Q. Shi, A. Okounkova, Dihao Sun, K. Watanabe, T. Taniguchi, James Hone, C.R. Dean[†], J.I.A. Li[†]

[†] Corresponding author. Email: cdean@phys.columbia.edu, jia.li@brown.edu

This PDF file includes:

Supplementary Text
Materials and Methods

THE INFLUENCE OF LAYER IMBALANCE

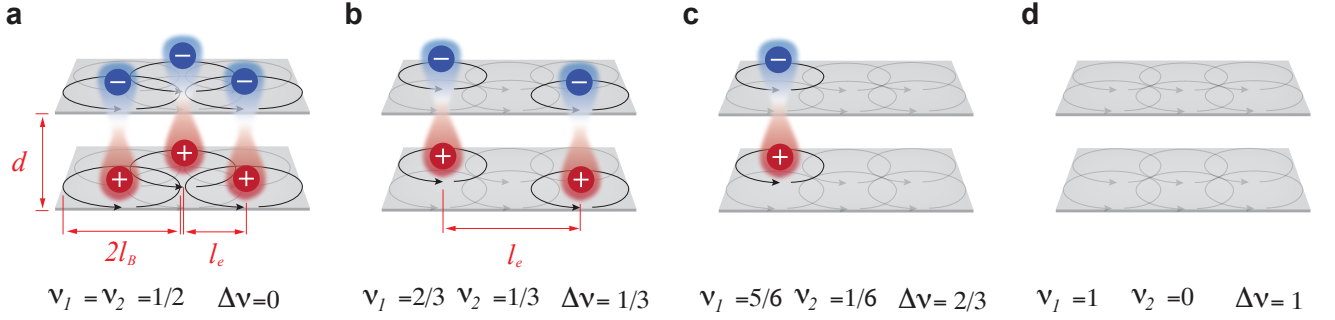


FIG. S1. **The excitonic density as a function of layer imbalance $\Delta\nu$** . Schematic diagram of interlayer excitons in a quantum Hall bilayer at $\nu_{total} = 1$. Black solid (gray) circles indicates occupied (unoccupied) Landau orbits. (a) Under layer-balanced condition, $\Delta\nu = \nu_1 - \nu_2 = 0$, interlayer excitons occupy half the available Landau orbital. As such, average spacing between excitons ℓ_e equals the average spacing between electrons, $\ell_e = \sqrt{\ell_B}$. In the presence of non-zero layer imbalance, the exciton density is reduced. For instance, excitons occupy 1/3 of Landau orbitals at $\Delta\nu = 1/3$ (panel b), whereas only 1/6 of the orbitals host excitons at $\Delta\nu = 2/3$ (panel c). In the limit of extreme layer imbalance, layer 1 and 2 are tuned to integer LL filling of $\nu_1 = 1$ and $\nu_2 = 0$. In this scenario, both layer are occupied by integer quantum Hall effect and the exciton density diminishes to zero. Taken together, the inter-exciton spacing can be defined based on layer imbalance $\Delta\nu$ as $\ell_e = \ell_B / \sqrt{1/2 - |\Delta\nu|/2}$.

Fig. S1 plots the schematic diagram of exciton density at different values of layer imbalance. Exciton density is maximized under the layer-balanced condition with $\Delta\nu = 0$ (Fig. S1a), giving rise to the smallest inter-exciton spacing $\ell_e = \sqrt{\ell_B}$. At extreme layer imbalance at $\nu_1 = 1$ and $\nu_2 = 0$ ($\Delta\nu = 1$), exciton density is zero. At an intermediate value of $\Delta\nu$, inter-exciton spacing is determined by $\ell_e = \ell_B / \sqrt{1/2 - |\Delta\nu|/2}$.

Fig. S4 plots the counterflow conductance, measured from a Corbino-shaped graphene bilayer (Fig. 1d), as a function of $\Delta\nu$ and T . While $\Delta\nu$ is varied from -0.8 to $+0.8$, ν_{total} is fixed at -1 . In the counterflow measurement, the presence of exciton pairing enhances the counterflow conductance G_{CF} , which is shown as red in the chosen color scale. Fig. S4a and b compares the $\Delta\nu - T$ map measured at two different d/ℓ_B -values. At $d/\ell_B = 0.63$ (Fig. S4a), a robust condensate phase occupy the layer imbalance range of $-0.6 < \Delta\nu < 0.6$. With increasing temperature, exciton pairing, evidenced by large counterflow conductance, persists to temperature much higher than the superfluid transition temperature T_c . This is consistent with the expected behavior in the strong-coupling limit of interlayer excitons [36]. At $d/\ell_B = 1.09$ (Fig. S4b), both the exciton condensate and excitonic pairing are limited to $T < 2$ K near the layer-balanced condition, which is in excellent agreement with the expected behavior in the weak-coupling regime [36]. However, strong exciton pairing is recovered at $d/\ell_B = 1.09$ by tuning the sample to the layer-imbalanced regime. In the range of $0.4 < |\Delta\nu| < 0.6$, both exciton condensate and exciton pairing persist to $T > 2$ K. The influence of $\Delta\nu$ on the temperature dependence of counterflow conductance is consistent with the observation in Fig. 2.

At $d/\ell_B = 1.09$, the single-layer FQHE states competes against exciton condensate near specific values of $\Delta\nu$. For instance, $\Delta\nu = -1/3$ corresponds to $\nu_1 = 1/3$ and $\nu_2 = 2/3$, where layer 1 and 2 are both occupied by the Laughlin state. The single-layer FQHE states is insulating in the counterflow measurements, which are shown as blue in the chosen color scale. On the other hand, the influence of this competition is negligible in the strong-coupling limit at $d/\ell_B = 0.63$.

EXCITON PAIRING STRENGTH

The strength of interlayer coupling is reflected by the onset temperature of exciton pairing, T_{pair} , relative to the superfluid transition T_c (Fig. S2a) [36]. In the strong coupling regime, exciton pairing survives to high temperature in the absence of the condensate. As such, T_{pair} is much larger than T_c in the presence of strong exciton pairing. In the weak coupling limit, exciton pairing and the superfluid condensate phase occurs simultaneously with decreasing temperature, $T_{pair} \sim T_c$. As such, the pairing strength can be characterized based on the size of the temperature window $\Delta T = T_c - T_{pair}$. T_{pair} is operationally defined as the temperature where Hall drag response exceeds a threshold of 20% the plateau value (Fig. S2a).

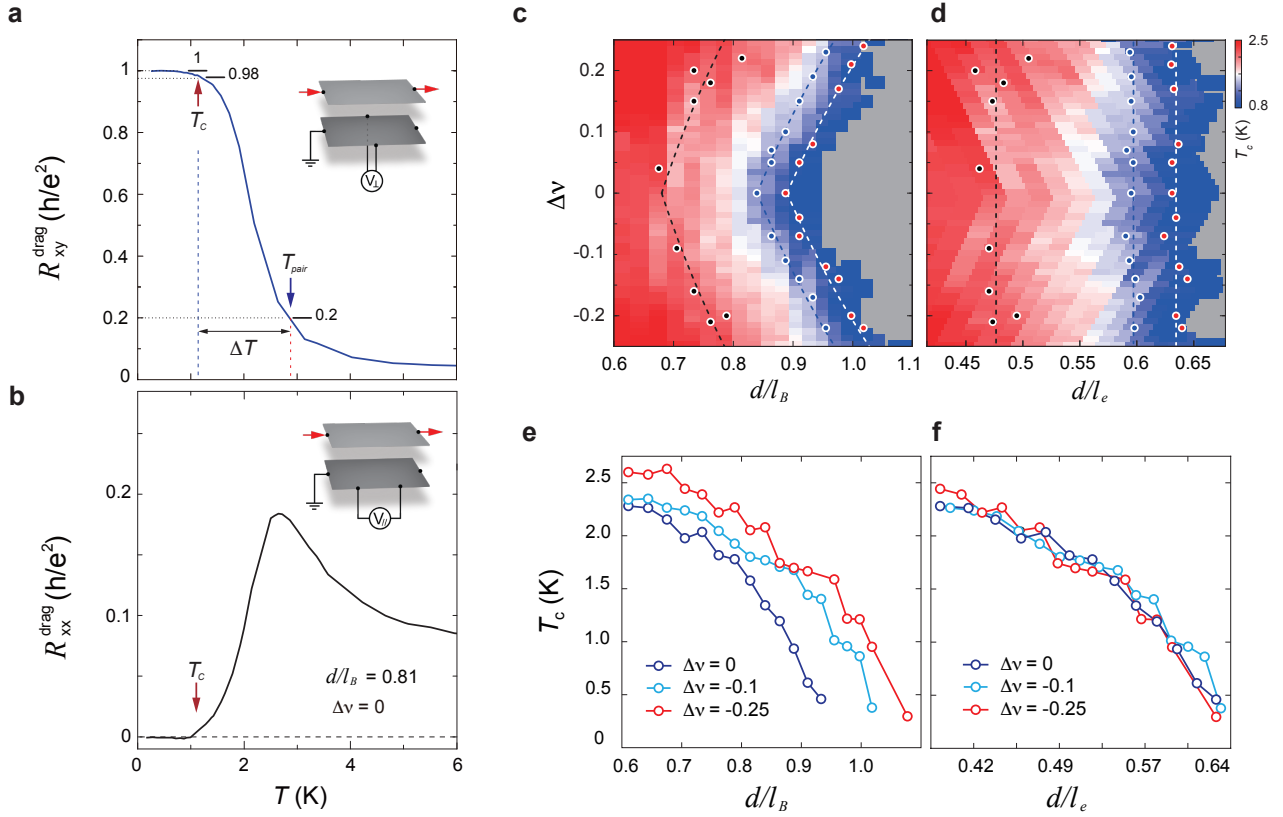


FIG. S2. T_c defined using longitudinal drag and Hall drag. (a) Hall drag R_{xy}^{drag} and (b) longitudinal drag R_{xx}^{drag} as a function of temperature T measured at $d/l_B = 0.81$ and $\Delta\nu = 0$. Inset shows the schematic diagram for Hall drag and longitudinal drag measurements. As shown in panel (a), T_c can be defined as the temperature at which Hall drag response equals 98% of the plateau value, $R_{xy}^{drag} = 0.98h/e^2$. Whereas T_{pair} is defined as the temperature at which Hall drag response drops to 20% of the plateau value, $R_{xy}^{drag} = 0.2h/e^2$. The temperature window ΔT denotes the difference between T_{pair} and T_c , $\Delta T = T_{pair} - T_c$. Similarly, T_c can be defined as the onset of longitudinal drag R_{xx}^{drag} with increasing temperature (panel b). Both definitions yields the same value for T_c . Panel (c-f) plots the dependence of T_c on d/l_B and d/l_e . T_c as a function of (d) $\Delta\nu$ and d/l_B , (f) $\Delta\nu$ and d/l_e . Constant values of T_c are marked by black, blue and red circles. T_c as a function of (e) d/l_B and (f) d/l_e measured at different interlayer density imbalance $\Delta\nu$. Here, T_c is defined as the temperature at which longitudinal drag R_{xx}^{drag} onsets from the noise floor with increasing temperature (marked by vertical red arrow in panel b). The dependence on d/l_B and d/l_e is in excellent agreement with the results shown in Fig.2, where T_c is determined based on the Hall drag response R_{xy}^{drag} .

Such a crossover behavior is shown in Fig. S5(a-b), which plots the Hall drag and longitudinal drag responses as a function of d/l_B and T . At small d/l_B , T_{pair} diverges to high temperature, whereas T_c remains around 3 K. This gives rise to a large ΔT , which is consistent with strong interlayer correlation in the strong coupling regime. With increasing d/l_B , both T_c and T_{pair} trend towards zero, which corresponds to a decrease in ΔT . A schematic phase diagram of T_c and T_{pair} is shown in Fig. S5c, where the bottom axis marks the evolution of excitonic pairing strength. The trend of T_c and T_{pair} resembles the BEC-BCS crossover phenomenon proposed by past theoretical works studying bosonic cold atom systems [69].

Similar to Fig. 2d-g, the value of ΔT is dependent on layer imbalance $\Delta\nu$. as shown in Fig. S3a, ΔT increases with increasing $-\Delta\nu$. At a given d/l_B . This suggests that d/l_B does not fully capture the excitonic pairing strength. On the other hand, replotting ΔT as a function of $\Delta\nu$ and d/l_e reveals that ΔT is independent of $\Delta\nu$ at a fixed value of d/l_e . As such, the excitonic pairing strength is fully determined by the ratio between d and l_e . The critical role of l_e , instead of l_B , provides an unambiguous evidence for a system of interacting excitons.

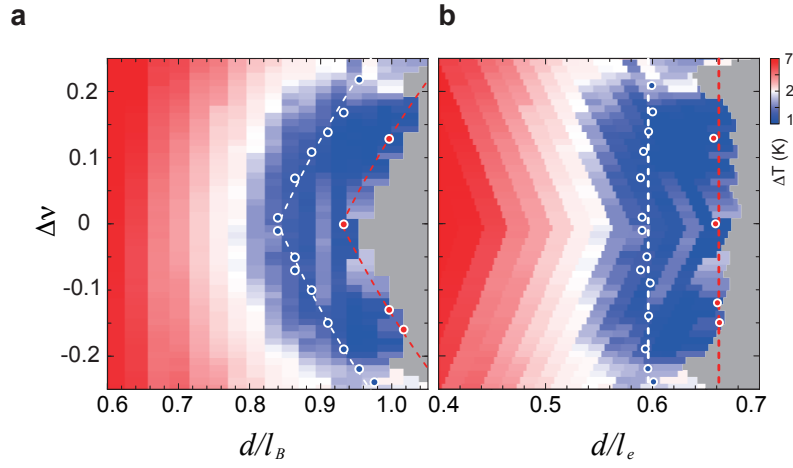


FIG. S3. ΔT as an indicator of excitonic pairing strength. ΔT is defined according to Fig. S2a. (a-b) ΔT as a function of $\Delta\nu$ and (a) d/ℓ_B , (b) d/ℓ_e . Blue and red circles mark constant values of ΔT . For a constant d/ℓ_B , ΔT increases with increasing $\Delta\nu$. Whereas ΔT is independent of $\Delta\nu$ for a constant d/ℓ_e . This indicates that the excitonic pairing strength is determined by inter-exciton spacing ℓ_e , instead of magnetic length ℓ_B .

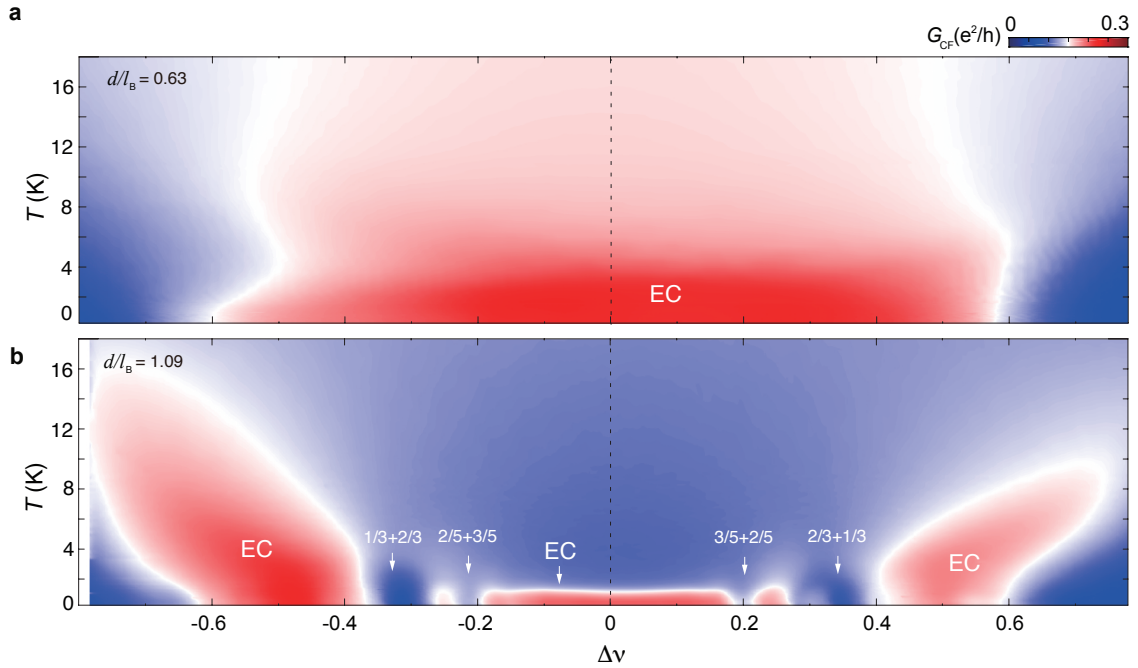


FIG. S4. The influence of $\Delta\nu$ on the exciton pairing strength. The counterflow conductance G_{CF} as a function of $\Delta\nu$ and T measured at (a) $d/\ell_B = 0.63$ and (b) $d/\ell_B = 1.09$.

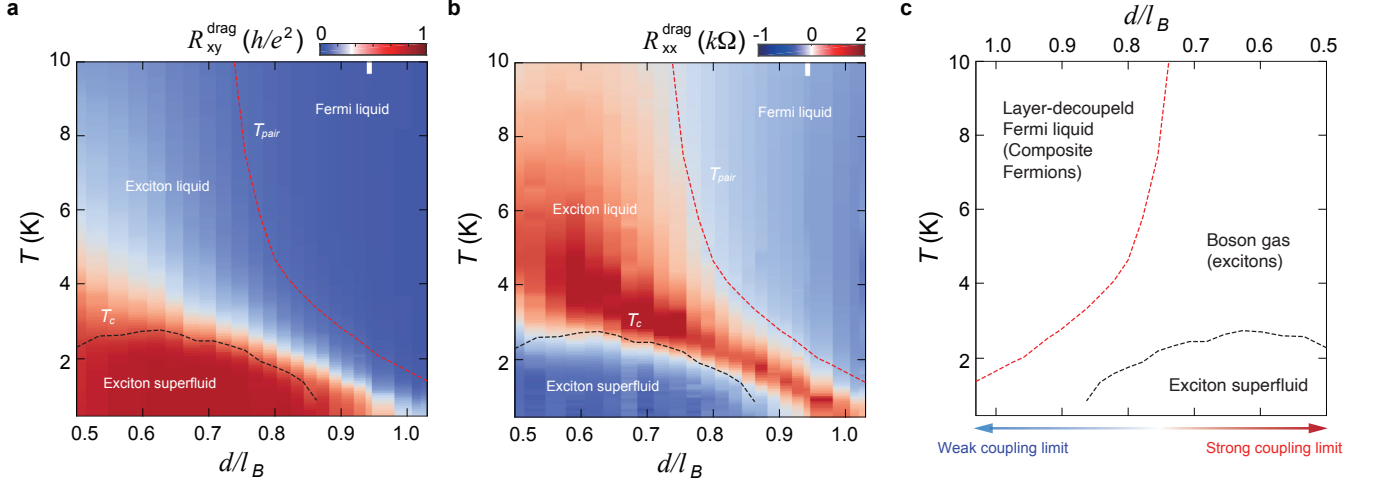


FIG. S5. **The crossover phenomenon with varying d/ℓ_B at $\Delta\nu = 0$.** (a-b) Coulomb drag measurement from a graphene double-layer sample shaped into a Hallbar geometry. (a) Hall drag and (b) longitudinal drag response as a function of temperature and d/ℓ_B when each layer is tuned to occupy half a Landau level at $\nu_1 = \nu_2 = -1/2$. The transition temperature of the condensate phase T_c is defined as the temperature where Hall drag response deviates from the quantized plateau, $R_{xy}^{\text{drag}} = h/e^2$. The dashed black line is operationally defined as the contour of constant Hall drag response of $R_{xy}^{\text{drag}} = 0.98h/e^2$. Along the same vein, the pairing temperature T_{pair} denotes the temperature where exciton pairing disappears. In this measurement, T_{pair} is operationally defined as the temperature where the Hall drag response becomes less than 8% of the quantization value. Red dashed line denotes T_{pair} , which is the contour line at a constant value of Hall drag response at $R_{xy}^{\text{drag}} = 0.08h/e^2$. (c) Schematic diagram demonstrating the crossover between the weak coupling and strong coupling limit by tuning d/ℓ_B (the value of d/ℓ_B is marked near the top axis).

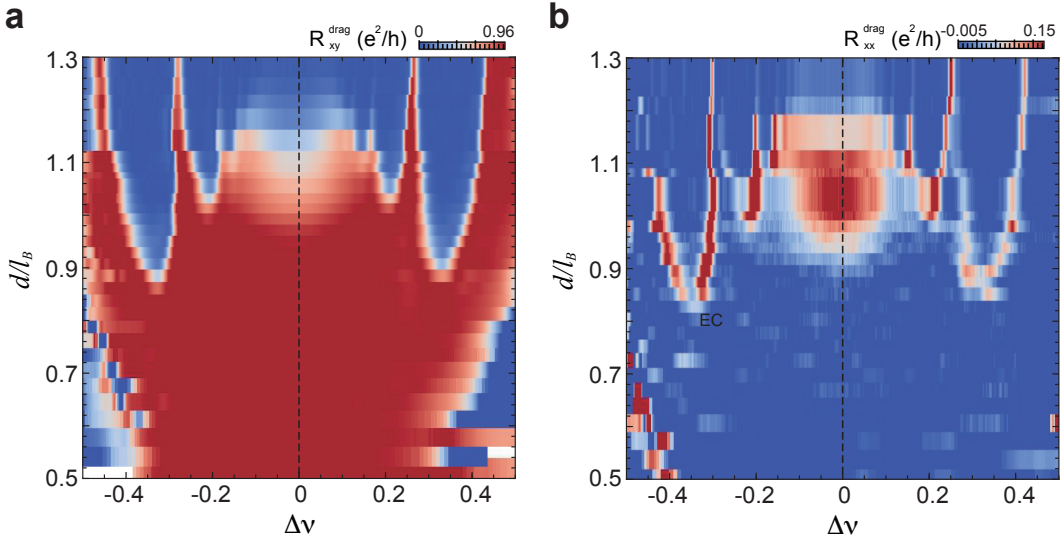


FIG. S6. **Coulomb drag measurement in Hall bar at $\nu_{\text{total}} = 1$** (a),(b) shows Hall resistance and longitudinal resistance in the drag layer as a function of $\Delta\nu$ and d/ℓ_B respectively. Both are measured at $T = 0.3$ K. The exciton condensate phase marked by unity Hall resistance and vanishing longitudinal resistance roughly occupies the same phase space as measured in corbino geometry shown in fig1(d) in the main text. (c) Hall resistance and longitudinal resistance in the drag layer versus d/ℓ_B when each layer is at half filling. (linecut in (a) and (b)) The maximum of longitudinal resistance coincide with $R_{xy}^{\text{drag}} = 0.5h/e^2$, in agreement with previous measurement in GaAs double quantum well[31]. The enhanced dissipative transport in drag layer could be explained by percolation model of two fluids[70, 71].

THE TRANSITION FROM THE EXCITON SOLID TO SINGLE-LAYER IQHE

As shown in Fig. S7, the transition from the exciton solid to the single-layer IQHE state coincides with a peak in the counterflow conductance. The location of this transition varies slightly depending on the direction from which the transition is approached (Fig. S7a). With increasing T , the solid-to-IQHE transition merges with the superfluid-to-solid transition at $T > 2$ K (Fig. S7b). As such, the solid-to-IQHE transition at low temperature can be determined by extrapolating the superfluid-to-IQHE transition from high temperature. This extrapolation is marked as white dashed lines in Fig. 3f-h.

In addition to the $\Delta\nu - T$ map, the transition between the exciton solid and single-layer IQHE states can also be determined based on the trajectory of the phase in the $\nu_{total} - \Delta\nu$ map. An exciton solid phase tracks $\nu_{total} = 1$, whereas single-layer IQHE state follows constant filling in a single layer (Fig. 2a-c). This provides an independent method to determine the location of the solid-to-IQHE transition.

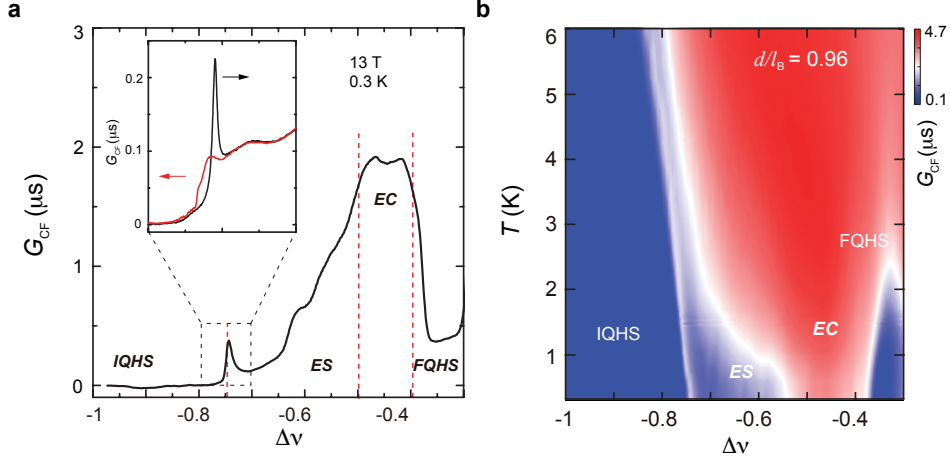


FIG. S7. **The phase boundaries of the exciton solid.** (a) Counterflow conductance G_{CF} as a function of $\Delta\nu$ measured from sample C1. The exciton solid occupies the range of $-0.75 < \Delta\nu < -0.5$, which is separated from the layer-decoupled IQHE state by a sharp peak in G_{CF} . The inset: G_{CF} is measured while $\Delta\nu$ is swept back and forth. Depending on the direction of the $\Delta\nu$ sweep, the transition boundary between the solid and IQHE states exhibits hysteresis. (b) Temperature-layer-imbalance ($T - \Delta\nu$) map of G_{CF} . The boundary between the exciton solid and IQHE states are marked by a peak in G_{CF} , which is shown as white in the chosen color scale. This phase boundary is consistent with the white dashed lines in Fig. 3f-h.)

| Name | d (nm) | Geometry |
|------|--------|----------|
| C1 | 7.4 | Corbino |
| C2 | 6.4 | Corbino |
| C3 | 3.9 | Corbino |
| C4 | 6.6 | Corbino |
| H1 | 7.4 | Hall bar |

FIG. S8. **List of devices used in this work** We used the data measured from the 5 representative devices in this work. The behavior of the rest of the devices aligns with these 5.

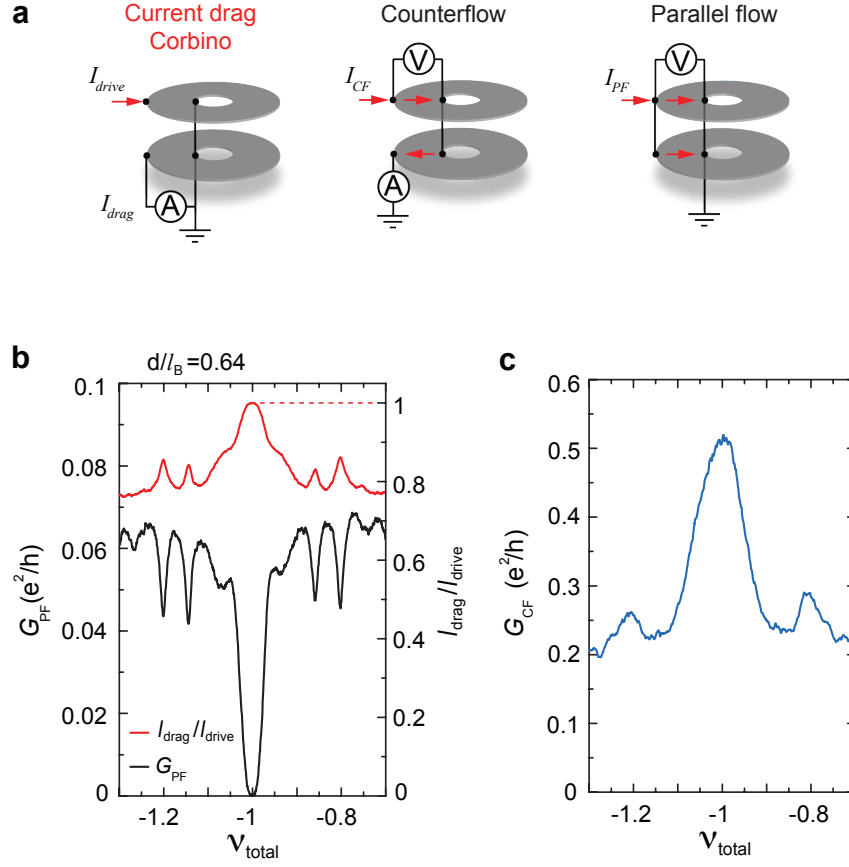


FIG. S9. **Transport measurement in the Corbino-shaped sample.** (a) Schematic diagram for different measurement configurations in Corbino-shaped samples. (b) Parallel flow conductance G_{PF} (black line) and the current drag ratio I_{drag}/I_{drive} (red line) as a function of total Landau level filling factor ν_{total} . The sample is under the layer-balanced condition throughout the measurement with $\Delta\nu = 0$. (c) Counterflow conductance as a function of ν_{total} . The existence of exciton condensate phase at $\nu_{total} = -1$ is evidenced by a combination of transport response: vanishing parallel flow conductance, perfect current drag with $I_{drag}/I_{drive} = 1$ and an enhanced counterflow conductance.

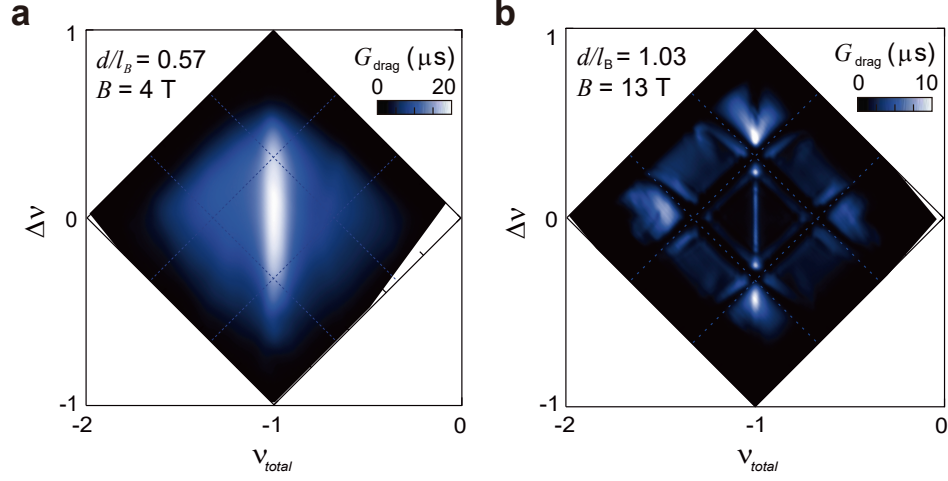


FIG. S10. $\nu_{\text{total}} - \Delta\nu$ map of counterflow conductance at $d/\ell_B = 0.57, 1.03$ The conductance measured in the coulomb drag configuration (analogous to the counterflow conductance) at $d/\ell_B = 0.57$ (a) and 1.03 (b) at $T = 0.3 \text{ K}$. In (a) the white stripe along $\nu_{\text{total}} = -1$ correspond to the exciton condensate phase where the conductance is maximum and bound by the contact resistance. (b) The dark checker board feature is the pattern of decoupled single layer fractional quantum Hall states, which is discussed in (cite double layer FQHE). The ground state at $\Delta\nu = \pm 1/3$, $\nu_{\text{total}} = 1$ has zero drag conductance, suggesting the ground state is decoupled FQHS. The dim color between $\Delta\nu = -1/3$ to $1/3$ along $\nu_{\text{total}} = 1$ suggests the absence of exciton condensate which agree with the drag ratio results shown in figure 1 in the main text.